FOI-R--0706--SE
November 2002
ISSN 1650-1942
User report

Environment assessment for underwater sensors in the Stockholm archipelago

Part 1 - Inversion of hydroacoustic sub-bottom parameters

Leif Abrahamsson

Brodd Leif Andersson

Ilkka Karasalo

Peter Sigray

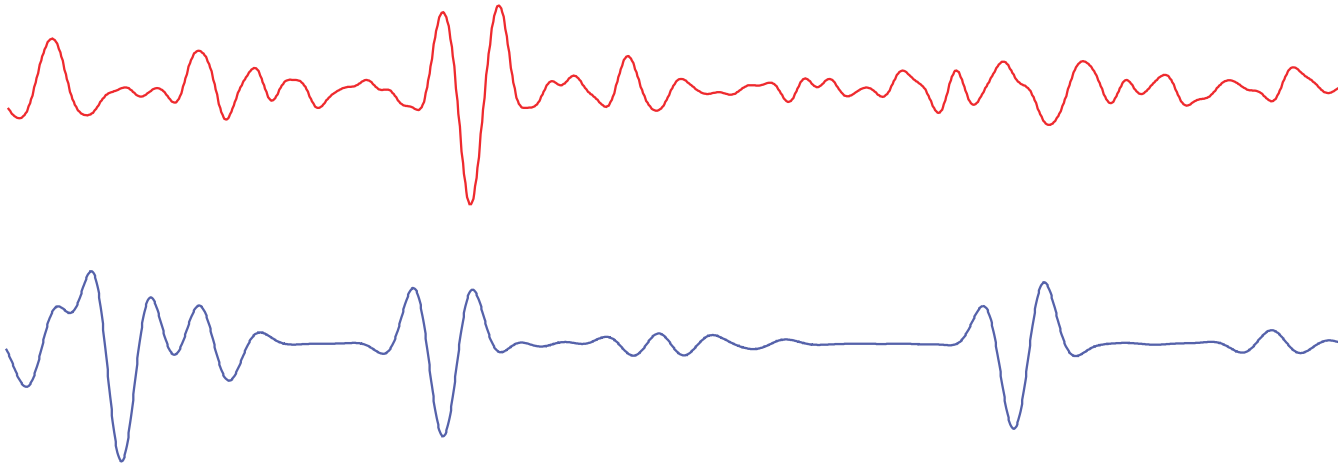

Systems Technology
SE-172 90 Stockholm

SWEDISH DEFENCE RESEARCH AGENCY

Systems Technology
SE-172 90 Stockholm

FOI-R--0706--SE

November 2002

ISSN 1650-1942

User report

Environment assessment for underwater sensors in the Stockholm archipelago

Part 1 - Inversion of hydroacoustic sub-bottom parameters

Leif Abrahamsson

Brodd Leif Andersson

Ilkka Karasalo

Peter Sigray

Issuing organization	Report number, ISRN	Report type
FOI – Swedish Defence Research Agency Systems Technology SE-172 90 Stockholm	FOI-R--0706--SE	User report
	Research area code 4. C4ISR	
	Month year November 2002	**Project no.** E6051
	Customers code 5. Commissioned Research	
	Sub area code 43 Underwater Sensors	

Author/s (editor/s)	Project manager
Leif Abrahamsson Brodd Leif Andersson Ilkka Karasalo Peter Sigray	Johan Mattsson
	Approved by Monica Dahlén
	Sponsoring agency Swedish Armed Forces
	Scientifically and technically responsible Leif Abrahamsson

Report title

Environment assessment for underwater sensors in the Stockholm archipelago
Part 1 - Inversion of hydroacoustic sub-bottom parameters

Abstract (not more than 200 words)

This report contains an inversion analysis of data recordings from a field trial in August 2002 in the Stockholm archipelago. The purpose of the experiment was to determine density, velocity and absorption of the seabed. Both the transmitter and the receiver were deployed on the seabottom with a separation distance of 13.2, 23.1 and 45.0 m. The emitted signals were Ricker pulses centered at the frequencies 0.5, 1, 2 and 4 kHz. The inversion is based on travel time analysis of echoes from the sediment interfaces. This analysis gave the following results. The depth to the bedrock is 17.3 m from the seabottom. It is covered by two sediments with the mean velocities 1425 and 1664 m/s and thicknesses 6.6 and 10.7 m. The density and absorption of the top sediment was estimated to 1500 kg/m^3 and 0.15 dB/λ and in the deep one to 1700 kg/m^3 and 0.1 dB/λ.

Keywords

Hydroacoustics, inversion, sub-bottom, parameters, Ricker pulse

Further bibliographic information	Language English
ISSN 1650-1942	**Pages** 31 p.
	Price acc. to pricelist

Utgivare Totalförsvarets Forskningsinstitut - FOI Systemteknik 172 90 Stockholm	**Rapportnummer, ISRN** FOI-R--0706--SE	**Klassificering** Användarrapport
	Forskningsområde 4. Spaning och ledning	
	Månad, år November 2002	**Projektnummer** E6051
	Verksamhetsgren 5. Uppdragsfinansierad verksamhet	
	Delområde 43 Undervattenssensorer	

Författare/redaktör Leif Abrahamsson Brodd Leif Andersson Ilkka Karasalo Peter Sigray	**Projektledare** Johan Mattsson
	Godkänd av Monica Dahlén
	Uppdragsgivare/kundbeteckning Försvarsmakten
	Tekniskt och/eller vetenskapligt ansvarig Leif Abrahamsson

Rapportens titel (i översättning)

Miljökarakterisering för undervattenssensorer i Stockholms skärgård
Del 1 – Inversion av hydroakustiska bottenparametrar

Sammanfattning (högst 200 ord)

Rapporten innehåller en inversionsanalys av mätdata från ett fältförsök i augusti 2002 i Stockholms södra skärgård. Syftet med försöket var att bestämma densitet, hastighet och absorption i bottensedimenten. Både sändare och mottagare placerades på botten med ett inbördes avstånd av 13,2, 23,1 och 45,0 m. De utsända signalerna var Rickerpulser med centerfrekvenserna 0,5, 1, 2 och 4 kHz. Inversionen bygger på gångtidsanalys av ekon från reflekterande gränsytor mellan sediment. Denna analys gav följande resultat. Berggrunden ligger på ett djup av 17,3 m från sjöbotten. Ovanför denna finns två sediment med medelhastigheterna 1425 och 1664 m/s samt tjocklekarna 6,6 och 10,7 m. Densitet och absorption i det översta skiktet uppskattades till 1500 kg/m^3 och 0,15 dB/λ och i det undre till 1700 kg/m^3 och 0.1 dB/λ.

Nyckelord

Hydroakustik, inversion, bottenparametrar, Rickerpuls

Övriga bibliografiska uppgifter	**Språk** Engelska
ISSN 1650-1942	**Antal sidor:** 31 s.
Distribution enligt missiv	**Pris: Enligt prislista**

Contents

1 Introduction

1.1 Background and purpose

This report contains an inversion analysis of acoustical data recorded in a field trial in August 2002 in the Stockholm Archipelago. The purpose of the experiment was to determine the density, sound velocity and attenuation of the sediments overlying the bedrock. The sediment thickness in the area could be several tens of meters [1]. The sediments covering the bedrock could be quite heterogeneous with layers of till, glacial and postglacial clays and a top layer of mud just beneath the seabottom [2]. The geoacoustical parameters of this structure strongly influence sound propagation in the water because sound waves will penetrate into the sediments and return to the water after reflections at sediment and bedrock interfaces. During the passage they will become weaker due to geometrical spreading, scattering and dissipation. Knowing the characteristics of the seabed is crucial for computing transmission loss in underwater acoustics.

Besides seabed characterization, this study is motivated by developing techniques for REA (Rapid Environmental Assessment). The purpose of REA is to determine critical environmental parameters in-situ from sonar data under operative conditions.

This work is part of an effort to integrate inversion results obtained from different points of departure. In the same field trial, several other experiments were carried out. An electromagnetic experiment was conducted with the aim to find the conductivities of the sediment layers [3]. A large acoustic and electromagnetic impedance contrast is present at the bedrock interface. This was detected by both the acoustic and electromagnetic inversions and the depth of the bedrock was found to be around 17 meters below the seabottom.

1.2 The seismic approach

Since the early 1920's seismic reflection techniques have been the most frequently used method to determine subsurface geological structures. Seismic marine geology is usually divided into three categories: vertical profiling, refraction and wide angle reflection techniques. This terminology is directly related to the main direction of propagation of the probing signals, vertical, horizontal or intermediate. The idea of the present experiment was to use a mix of all three. The transmitter and receivers were deployed on the seabottom. A reference hydrophone was mounted on the same platform as the transmitter to account for near vertical bottom returns. The direct wave between the source and receiver travels horizontally and picks up acoustical information of the seafloor. After the arrival of the direct wave follow reflections from sediment interfaces. From their arrival times layer velocities and thicknesses can be inferred. Although this experiment mimics reflection seismics, the scale of operations is small compared to traditional marine seismic work. A conventional piezoelectric transducer was employed, while towed, energetic signal sources like airguns or sparkers are utilized in seabed mapping of large areas. The static configuration with bottom mounted transmitters and receivers has some important advantages though. This setup circumvents modeling difficulties in dealing with the sound velocity profile of the water, since first order

reflections arriving at the receiver have traversed sediments only. Moreover, it excites lateral waves, which carry distinct information of the seafloor. The proximity to the bottom permits the use of a low-power transmitter with the ability to emit most any pulse form. In this experiment the transmitted waveforms were Ricker pulses centered at the frequencies 0.5, 1, 2 and 4 kHz.

1.3 Summary of inversion results

A strong reflector, most likely the bedrock, was found at a depth of 17.3 m from the seabottom. The sediment above consists of two layers with thicknesses 6.6 and 10.7 m. The mean velocities of these layers are 1425 and 1664 m/s. The velocity of the top sediment varies appreciably by depth. At the seafloor the velocity is 1390 m/s, while it could be as large as 1575 m/s at the interface with the deep sediment. There is evidence that the surface layer of the sediment forms a sound channel, which extends from the seafloor to a depth of several meters. The details of the velocity profile are uncertain.

The impedance of the seafloor was found to be $2.1 \cdot 10^6$ kg/m^{2}s at 1-2 kHz. The attenuation of the top sediment is 0.15 dB/λ, while it is somewhat less in the deep sediment. The densities of the sediments are 1500 and 1700 kg/m^3.

The sediment interfaces are diffuse with a transition zone and roughness that could be on a scale of several meters. Scattering due to interface roughness, and most likely volume inhomogeneities as well, is the main cause of fading reception by range of echo levels from the deep bedrock interface at frequencies larger than 1 kHz. The transmisson loss of the 500 Hz signal was much less, but the weak power output of the source (137 dB) was a limiting factor. There are no results on the origin of the scattering phenomena due to lack of adequate modeling tools. Nor do the models in this work account for lateral variations of the seabed. The consequences of these shortcomings will be discussed in Sec. 7 and 8.

The inversion analysis of the recordings has followed three lines: travel time analysis, lateral wave analysis and deductive reasoning based on observations and theory. Attempts to automatize the inversion by search algorithms were beset with difficulties, which require further efforts to be resolved.

The full inversion result is listed in Sec. 7.4, which also contains graphical comparisons between model results and measurements.

1.4 Relations to previous work

In May 2001 an acoustical inversion experiment was conducted in the same area with a quite different technique [4]. The objective was to find so-called equivalent media parameters, which would be good enough for model predictions of the transmission loss in the sea. It is natural that such simplified environmental descriptions may be nonunique and frequency dependent. Nevertheless, it might serve well for its purpose. This inversion was based on transmission loss data taken along a 3 km linear track, see map on page 3. The source was towed along the track and the transmitted signal was recorded by a vertical array of hydrophones. The frequency range of the emitted

signals was from 75 to 375 Hz.

The purpose of the experiment in August 2002 was to find ground truth, that is the actual values of geoacoustical sub-bottom parameters. Therefore both the transmitter and receivers were bottom located to improve the excitation and reception of waves in the seabed. The emitted signals were short pulses and the inversion was based on echo analysis. Comparisons and evaluations of both approaches is a topic for future research.

2 The field trial

2.1 The test site

Horsfjärden is an area with varying sedimental properties. In the southern part, near to Adamsskären, the sediment is soft and claylike and the crystalline bedrock is expected to be situated deep under the sea-bed. Somewhat north, between Käringholmen and Vitsgarn, the crystalline bedrock rises so to constitute the two islands. It is expected that the clay layer is thinner here, and that the bedrock is to be found nearer to the seabed. Due to their sedimental properties both places were chosen for the trials. They are marked by Urd 1 and Urd 2 in the map below.

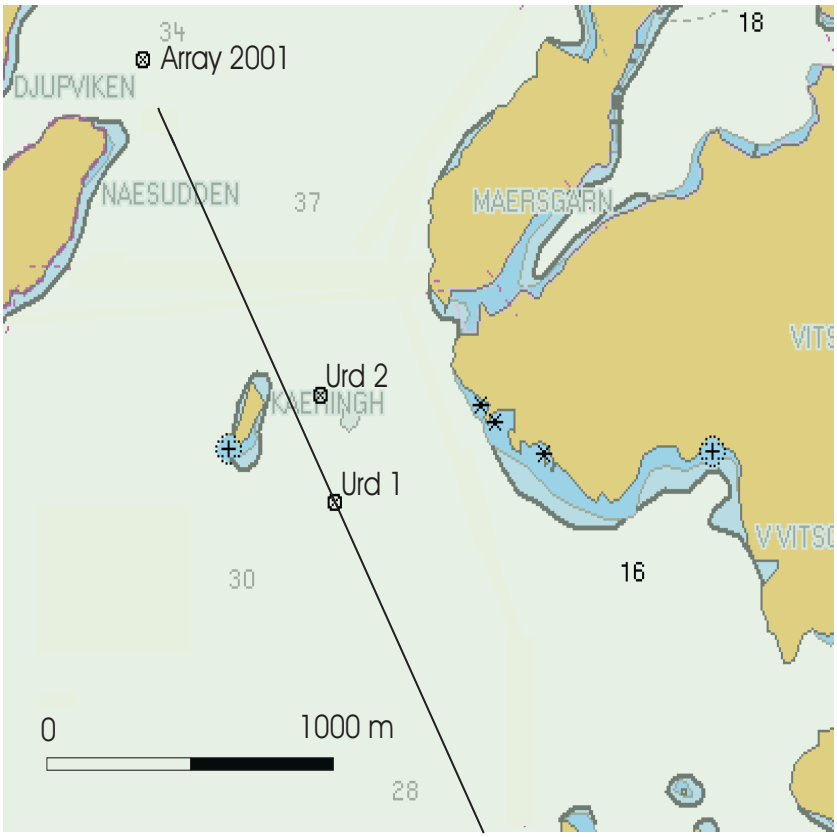

Figure 2.1: Map of Horsfjärden. The sites of the measurements are denoted by Urd 1 and Urd 2. The black line is the track in the May 2001 field trial.

The sound velocity profile was measured several times during the experiment. The velocity conditions were stable. The velocity was constant down to 7-8 meters and then decreased linearly down to the bottom. The measured sound velocity profiles are shown in Fig. 2.2 together with the profile used in the model runs.

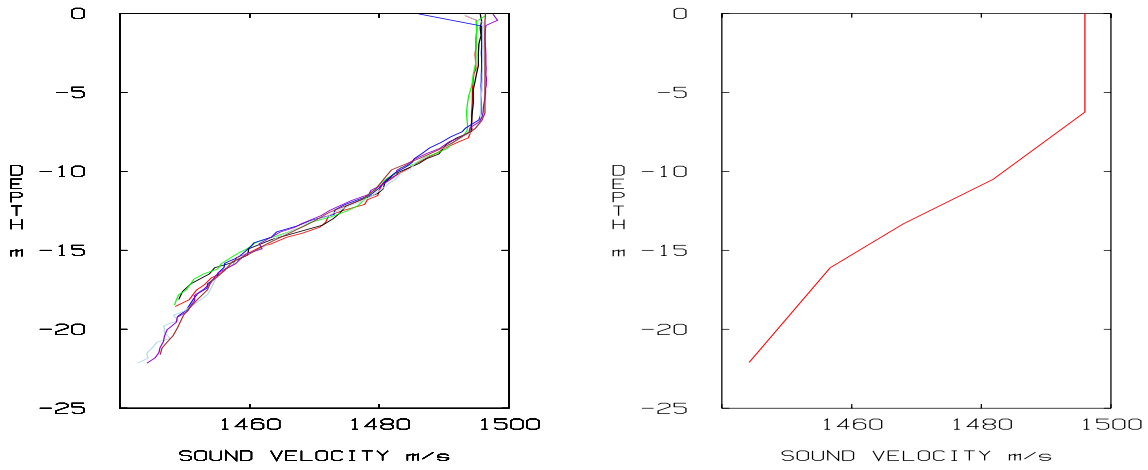

(a) Sound velocity profiles measured during the August 2002 trial in Djupviken.

(b) Sound velocity profile used in the model runs.

Figure 2.2: Sound velocity profiles at the test site.

The experiment took place during two days in the end of August 2002. The first day the wind speed was about 0-3 m/s, the second day about 10-12 m/s.

In the following we shall deal only with the measurements at the northern test site Urd 2.

2.2 Experimental setup

The ship HMS Urd was used for the trials. The ship was anchored at the test site. In order to avoid unnecessary interference from the ship, it was put into a silent mode. The measuring system consisted of three units, the transmitter, the receiver and the digital acquisition system (DAS). The transmitter unit was constructed on a triangular plastic frame, carrying the transmitter and the reference hydrophone. The latter was used for an independent check of the transmitted signal. Unfortunately, acoustic energy was transmitted not only through the water but also mechanically by the frame, from the transmitter to the reference hydrophone, hereby giving rise to an oscillatory behaviour super-imposed on the signal of interest. The unwanted oscillations ceased after 5-25 ms depending on the frequency of the transmitted signal. This misfortune was partly the reason for using the receiver hydrophone for most of the subsequent analysis. The transmitter was of the spherical variety with a maximal transmission at 10 kHz (manufactured by Bruel & Kjaer ORTS1013). In the trials the transmitter was deployed on the seabottom at the aft of the ship and thereafter kept stationary during the whole measurement period. The receiver was a Bruel & Kjaer 8101 hydrophone. The frequency response was flat from 200 Hz up to 20 kHz. The equipment was designed to

enable smooth deployment and retrieval. The receiver hydrophone was also deployed on the seabottom at distances 13.2, 23.1 and 45.0 m from the transmitter. These distances were calibrated after the trial using the arrival times of the direct wave between the source and receiver and the velocity of the water at the bottom. At the site these distances were crudely measured by a rope from the ship to be around 10, 20 and 40 meters.

The water depth was measured at the ship to 22.5 m. In our models we have assumed that the bottom is flat, although an analysis of arrival times of air/water reflections at the receivers, reveals that the water depth at the receivers may differ within one meter.

All receivers and the transmitter were calibrated before and after the trials. The DAS was placed in the wheel-house. Cables were placed carefully on deck as to avoid interference. Before A/D conversion, signals where low-pass filtered to avoid aliasing. Apart from the acoustic signals the output of the transmitting amplifier was recorded as well.

2.3 Transmitted waveforms

All probing signals in the experiment were Ricker pulses centered at the frequencies 0.5, 1, 2 and 4 kHz. It means that the durations of the source pulses were around 2, 1, 0.5 and 0.25 ms. The original Ricker pulse is defined by

$$r(t) = -\frac{2}{\sigma^2}(t^2 - \frac{1}{2}\sigma^2)e^{-\frac{t^2}{\sigma^2}}, \quad -\infty < t < \infty, \tag{2.1}$$

where t is time in seconds. The function (2.1) is the second derivative of the Gaussian function. It is normalized such that its peak value at $t = 0$ is $r(0) = 1$. The parameter σ (dimensions of time) is used to control the pulse width, or equivalently the bandwidth. It is common to specify $\sigma = 1/(\pi f_c)$, where f_c is the center frequency of the pulse. This fact can be derived from the Fourier transform $\hat{r}(\omega)$ of $r(t)$:

$$\hat{r}(\omega) = \omega^2\sigma^2\frac{\sqrt{\pi}}{2}e^{-\frac{\omega^2\sigma^2}{4}}.$$

It can also be verified from the analytic form (2.1) that $1/f_c$ is a good approximation of the pulse length. The Ricker pulse with f_c= 2 kHz and a modified version are displayed in Fig. 2.3. The latter is quite similar to the autocorrelation of the Ricker pulse, although it was designed differently by B-splines [5]. Their normalized energy spectra are shown in Fig. 2.4.

In the modified pulse the ratio of positive and negative pressure peak values is smaller, which raises the energy by some 25 percent. Since source power is a main concern in transmitting acoustic signals deeply into absorptive media, the modified Ricker pulse has been used throughout this experiment. For brevity though, we shall omit the attribute 'modified', and simply refer to the source pulse as a Ricker pulse.

The Ricker pulse was chosen because it has a nearly optimal time·bandwidth product (a pure Gaussian would be). This is a computational advantage when time-dependent solutions are synthezised from frequency-domain solutions by the discrete Fourier transform. All our wave propagation codes are based on this approach. For efficiency reasons

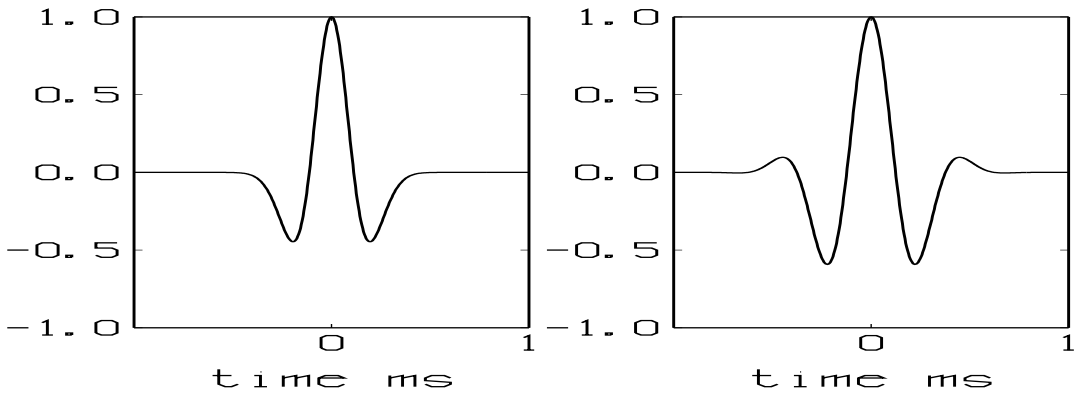

Figure 2.3: The Ricker pulse (left) and its modified version (right) centered at the frequency 2 kHz.

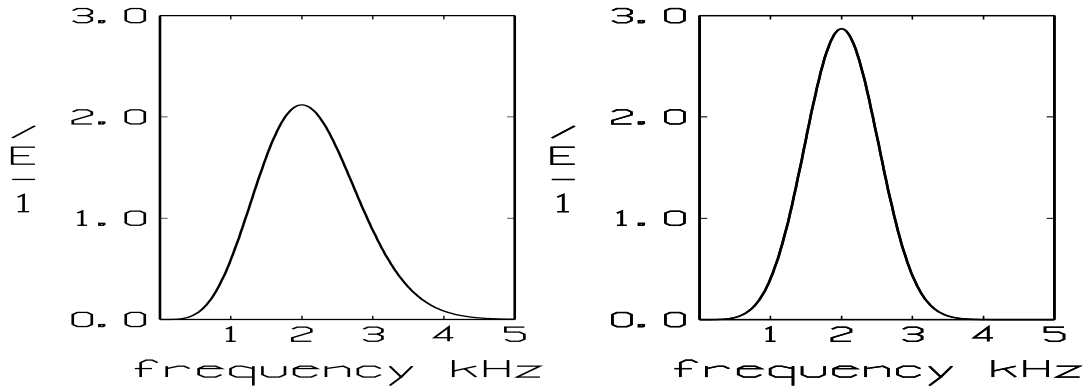

Figure 2.4: Normalized energy spectra of the Ricker pulse (left) and its modified version (right). The pictures show that both pulses have largest energy at 2 kHz.

the number of frequencies needed to assemble the time-series should be kept at a minimum. For a given pulse length, the Ricker pulse has a smaller bandwidth than most any other waveform.

The source strengths measured by peak values in the reference hydrophone were 137, 147, 157 and 167 dB re 1 μPa for the Ricker pulses centered at 0.5, 1, 2 and 4 kHz respectively. The increase of the source power by frequency implies that the emitted pulse shape disagrees with the desired one. However, by looking at measured waveforms, the distortions seemed to be so insignificant that the source in our models need not be adjusted.

3 Signal processing of measured data

The sampling rate of the received signals was 30 kHz, and 6000 samples were kept for each pulse, comprising a recording time of 200 ms. The pulse was repetively transmitted 100 times in two sessions with different pulse repetition frequencies. In the first set the pulses were emitted at a rate of 2.9 Hz and added coherently at collection time. In the second set the ping rate was 0.31 Hz and all pings were stored on file. After

the trial they were stacked upon each other without any prior time alignment relying on perfect synchronization of the electronics. The final signals from the two sets were found to agree fairly well, although there are some notable exceptions. Time intervals in which significant departures occur were sorted out before the inversion analysis. Fig. 3.1(top) shows a typical appearance of a received signal from one ping. There are two conspicuous disturbances: a strong dc bias and a 50 Hz wave. The latter presumably originates from the power generator on board HMS Urd. The result of stacking and translation to remove dc is shown in Fig. 3.1(bottom).

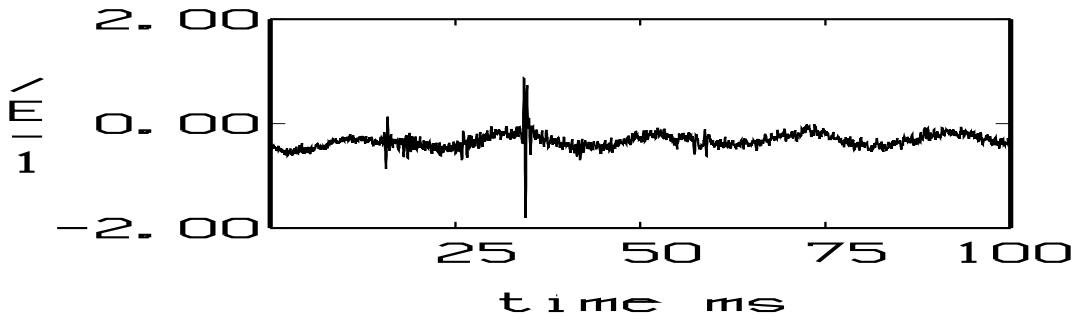

(a) a single ping

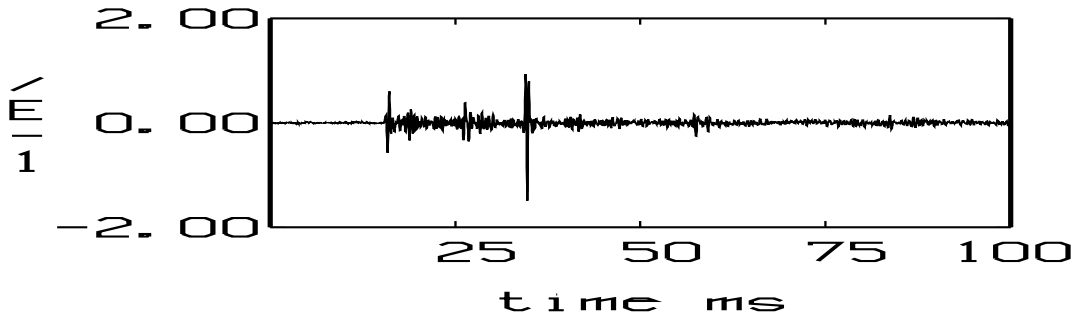

(b) 100 pings stacked coherently

Figure 3.1: Example of ping (unnormalized) of a 2 kHz Ricker pulse received at 23.1 m (top). Mean of 100 pings and after removal of dc bias (bottom).

3.1 Bandpass filtering

The spectrum of the signal in Fig. 3.1(bottom) is shown in Fig. 3.2. It should be compared to the spectrum of the source pulse in Fig. 2.4(right).

The 50 Hz signal is still present in the stacked signal besides some low-frequency components that did not vanish by averaging. As a consequence bandpass filtering was

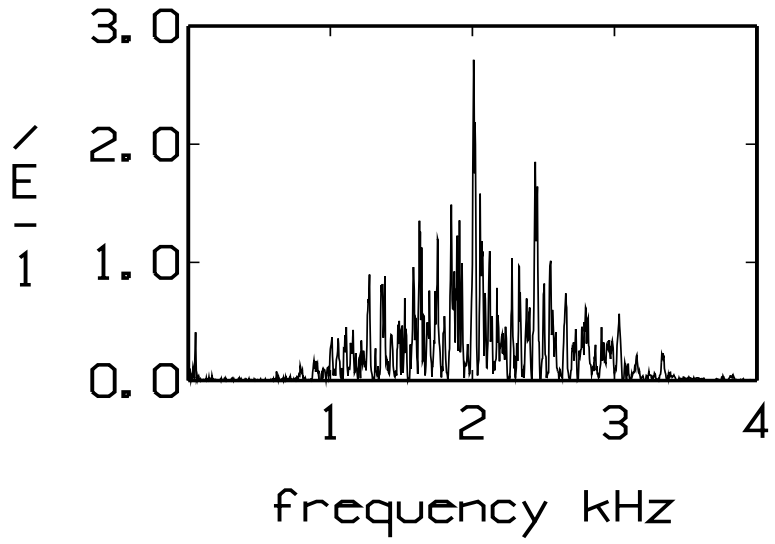

Figure 3.2: Energy spectra of the signal shown in 3.1(bottom). Normalized to be comparable with Fig. 2.4

applied with a transfer function

$$H(f) = \begin{cases} 1 & B_2 \le |f| \le B_3 \\ 0 & |f| \le B_1 \text{ and } |f| \ge B_4 \\ \le 1, \text{ (smooth rolloff by B-splines)} & B_1 \le |f| \le B_2 \text{ and } B_3 \le |f| \le B_4 \end{cases} \tag{3.1}$$

The corner frequencies B_i were chosen such that merely a tiny part of the source spectrum was affected. The actual choice is listed in Tab. 3.1.

Ricker pulse center freq Hz	bandpass corner frequencies, Hz			
	B_1	B_2	B_3	B_4
500	75	125	1000	1125
1000	75	150	2000	2250
2000	150	250	4000	4500
4000	250	500	8000	9000

Table 3.1: Filter coefficients in transfer function (3.1).

3.2 The signal envelope

In the received signal it is observed that bottom returns appear as localized wave trains unlike the emitted pulse. An explanation might be presence of interface roughness or transition zones, which extend over several wavelengths. Then the incident wave will undergo a series of reflections with additional diffraction effects depending on the

wavelength. The interaction time at such a boundary could well exceed the pulse width and the return will be spread in time with an unpredictable waveform. Then it is more appropiate to look at the energy of the signal rather than the wave amplitude. In practice this can be realized by forming the envelope of the signal [6]. Let $p_r(t)$ denote the recorded time series and $h_r(t)$ its Hilbert transform. Then the envelope squared $E_r(t)$ is given by

$$E_r(t) = p_r^2(t) + h_r^2(t). \tag{3.2}$$

We shall normalize this energy by the peak value of the corresponding energy at the reference hydrophone. By taking 10log of the normalized signal envelope squared, we obtain the usual transmission loss in dB as a function of time. For convenience this function is simply called the signal envelope. Fig. 3.3 illustrates the difference between the amplitude and envelope wave forms. As can be seen, the envelope offers a simplification at the expense of loss of phase information. In this study we will need to deal with both forms depending on the importance of pulse shapes.

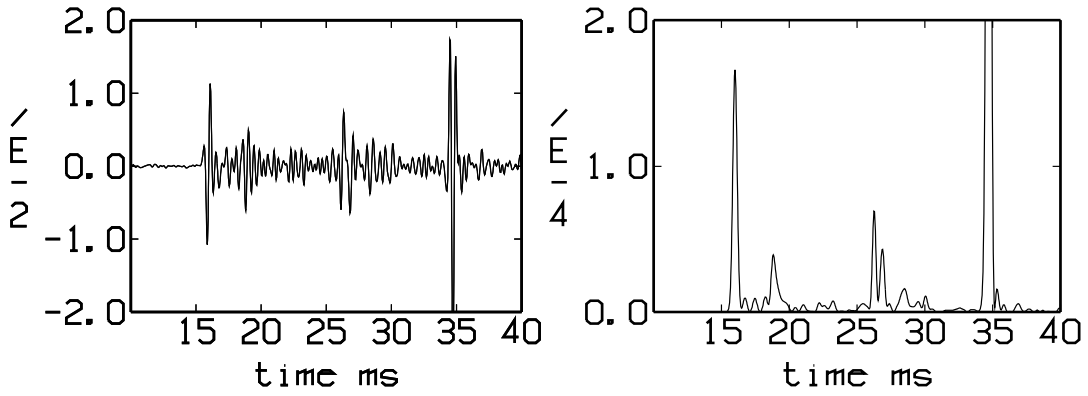

Figure 3.3: Recordings of normalized pressure amplitude versus time at the receiver at 23.1 m (left). The signal envelope of the pressure pulse at 23.1 m (right). The center frequency of the Ricker pulse is 2 kHz. The direct and the surface reflected waves appear at 16.0 and 34.5 ms respectively.

4 Modeling tools

The input to a wave propagation model is a set of acoustical parameters associated with a geometric description. The output is a computed pressure wave that signifies the wave response of the given media to the the signal source of the model. The basic idea of inverse modeling is to adjust the parameters of the model until a satisfactory fit between modeled and measured curves is achieved. This process is usually automated by using an optimization algorithm.

Another equally important aspect of modeling is training to recognize typical wave features like the response of hard/soft media etc. Such insights are helpful in the planning of experiments, and makes it possible to visually identify reflectors of interest

by direct readings of data recordings. In exploration seismology as practiced by the petroleum industry, this is a profession by itself [7].

In this work several computational models have been employed. A brief account of the models and software follows below.

MODE-I Modified version of MODELOSS [8] for inversion analysis. Based on normal-mode expansions. Applicable to far-fields only. Transmission into semi-infinite bedrock not accounted for. CPU: one second/ kHz/layer.

RAY-I Modified version of raytracing program in MUMS [9]. Computes eigenrays between two points on the seabottom. Output includes travel time, refraction angles, separate loss factors due to geometry, reflection/refraction, absorption and traces for preselected raypaths. Lateral waves by option. CPU: one second/100 rays.

LWAVE-I Computes the sound field for a monopole source on the interface between two semi-infinite, homogeneous media. The solution is expressed as a Sommerfeld integral (6.1), which is evaluted by numerics borrowed from NLAYER [10]. Used in this report to explore the properties of lateral waves. CPU: one second/kHz.

XFEM_S Computes the full wavefield from a mono-frequency source in a range-independent layered fluid-solid medium by a Hankel-Bessel transform integral method. Uses an adaptive high-order integration method for the transform integrals [11] and a node-free finite element technique based on exact finite elements [12] for solving the two-point boundary value problem for the field as function of depth at fixed horizontal wavenumber.

All these codes assume that layers are plane and horizontal with acoustical parameters varying by depth only. All codes accept both monofrequency and pulsed sources. Time-dependent solutions are synthezised from frequency-domain solutions by the discrete Fourier transform. Except for RAY-I, in practice there is an upper limit $\approx$ 10 kHz on the frequency being used.

5 Travel time analysis

The velocities and thicknesses of a sequence of horizontal, plane layers can be determined by curves of reflection travel times versus horizontal range. For the first layer this curve is a hyperbola and the velocity can be found by Green's method [13]. The multiple layer case can be reduced to Green's method by a top-down, layer by layer approach in which the reflection curve for a layer is compensated for time delays due to layers above. The mathematical theory was worked out by Dix [14]. This approach is called the wide angle reflection technique in seismic marine geology. It is usually applied to data at densely spaced points in range. In the present experiment we shall make use of data at just two receivers. For the two-layer case this leads to a 4 by 4 system of equations, that is derived in Sec. 5.1. The result of solving these equations after supplying observed arrival times is presented in Sec. 5.2.

5.1 Theoretical background

We start to consider the case of one sediment with thickness H_1 and velocity c_1. Let L_1 and L_2 be the horizontal ranges (offset) between the receivers and the source, and let t_{11} and t_{12} be the arrival times at L_1 and L_2, see Fig. 5.1. Then the distances traveled by the waves reflected at the bottom of the layer satisfy the equations

$$\sqrt{L_1^2 + 4H_1^2} = c_1 t_{11}$$
$$\sqrt{L_2^2 + 4H_1^2} = c_1 t_{12}$$

For known values of t_{11}, t_{12}, L_1, L_2, the solution to this system is given by

$$c_1 = \sqrt{\frac{L_2^2 - L_1^2}{t_{12}^2 - t_{11}^2}}, \quad H_1 = \frac{1}{2}\sqrt{c_1^2 t_{11}^2 - L_1^2}. \tag{5.1}$$

It should be noted that the computed velocity becomes sensitive to disturbances in the arrival times t_{11} and t_{12} for small time separations $t_{12} - t_{11}$. More precisely, by differentiation of the expression (5.1) for the velocity we obtain

$$\frac{dc_1}{c_1} \approx -\frac{1}{2}\frac{dt_{12} - dt_{11}}{t_{12} - t_{11}}$$

which implies that $t_{12} - t_{11}$ must be considerably larger then the errors in the recordings of the arrival times. As a consequence, the range separation $L_2 - L_1$ between the receivers must not be too small compared to the layer thickness because

$$t_{12} - t_{11} \approx \frac{L_2 - L_1}{c_1} \cdot \frac{L_2 + L_1}{4H_1}$$

for $H_1 > \frac{1}{4}L_2$.

By the same reasoning, with the roles of L_2 and H_1 reversed, the time separation diminishes when offsets are large compared to layer thickness. At large ranges the reflected wave would merge to some extent with the direct one depending on the duration of the emitted pulse. Additional difficulties with long ranges may be weak reception and environmental variations by range. In conclusion, travel time analysis requires a judicious choice of source-receiver ranges. An offset of the order 2-3 layer thicknesses appears to be adequate. However, proper account must also be taken to the source characteristics and media absorption. Using short pulses improves resolution until reception is lost due to scattering and absorption.

Next consider the case of two horizontal and flat sediments with thicknesses H_1 and H_2 and velocities c_1 and c_2. These parameters can be determined by four arrival times t_{11}, t_{21} at L_1 and t_{12}, t_{22} at L_2, see Fig. 5.1. As before, c_1 and H_1 are found by the formulas (5.1) using t_{11} and t_{12}. The remaining equations for c_2 and H_2 also involve the grazing angles θ_1 and θ_2 at the source of the two departing rays headed for the receivers at the ranges L_1 and L_2. These rays traverse both layers twice. We shall use the notation

$$x = \cos\theta_1, \quad y = \cos\theta_2, \quad q = \frac{c_2}{c_1}.$$

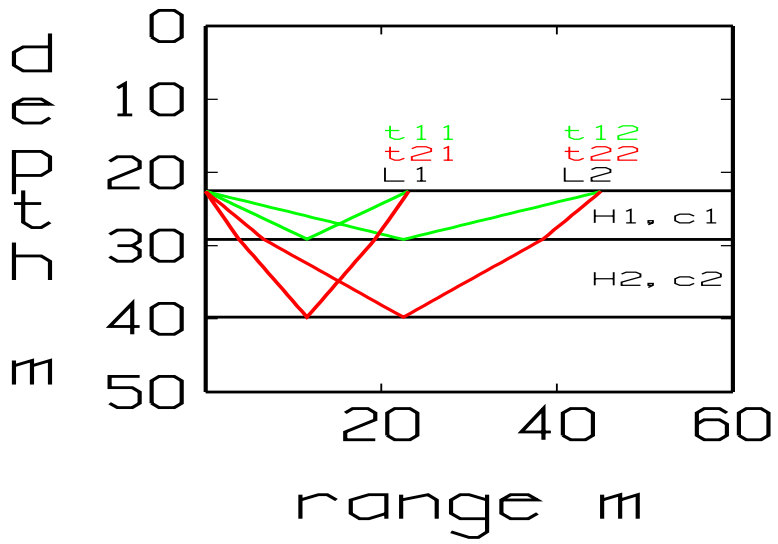

Figure 5.1: Eigenrays traversing one sediment (green) and two sediments (red) with source and receivers (L_1, L_2) at the seabottom

Then the cosine of the grazing angles in the deepest sediment are qx and qy according to Snell's law. Considering the geometry and traveling times of the two ray paths, the following set of equations for x, y, q, H_2 can be set up:

$$\frac{H_1 x}{\sqrt{1-x^2}} + \frac{H_2 q x}{\sqrt{1-q^2x^2}} = \frac{L_1}{2} \tag{5.2}$$

$$\frac{H_1 y}{\sqrt{1-y^2}} + \frac{H_2 q y}{\sqrt{1-q^2y^2}} = \frac{L_2}{2} \tag{5.3}$$

$$\frac{H_1}{\sqrt{1-x^2}} + \frac{H_2}{q\sqrt{1-q^2x^2}} = \frac{c_1 t_{21}}{2} \tag{5.4}$$

$$\frac{H_1}{\sqrt{1-y^2}} + \frac{H_2}{q\sqrt{1-q^2y^2}} = \frac{c_1 t_{22}}{2} \tag{5.5}$$

The first two equations (5.2-3) can be conceived as conditions on the departure angles θ_1 and θ_2 so that the rays will return to the horizon at L_1 and L_2. The last two equations (5.4-5) are the usual travel time-distance-velocity relationships for the two rays.

The system (5.2-5) is a nonlinear system of equations which can be solved by Newton's method, at least if the velocity contrast q is not too large. Then a good initial approximation is provided by putting $q = 1$. This is equivalent to a least-distance raypath instead of the correct least-time according to Fermat's principle.

5.2 Inversion results based on traveling time

Next we look at the recordings and try to identify echoes from sediment interfaces. To begin with we shall use only the time series at $L_1 = 23.1$ m and $L_2 = 45.0$ m simply

because they are more distinct than those at 13.2 m and the reference hydrophone. Inspection of data suggests that there are two major arrivals at each location as follows:

$$\begin{array}{ll} t_{11} = 18.6 \text{ ms} & L_1 = 23.1 \text{ m} \\ t_{21} = 26.4 \text{ ms} & L_1 = 23.1 \text{ m} \\ t_{12} = 32.9 \text{ ms} & L_2 = 45.0 \text{ m} \\ t_{22} = 36.0 \text{ ms} & L_2 = 45.0 \text{ m} \end{array} \tag{5.6}$$

These arrivals are easy to recognize because they appear between the arrivals of the direct and the surface reflected waves. A series of snapshots of the envelope of the signal at $L_1 = 23.1$ m and $L_2 = 45.0$ m is shown in Fig. 5.2.

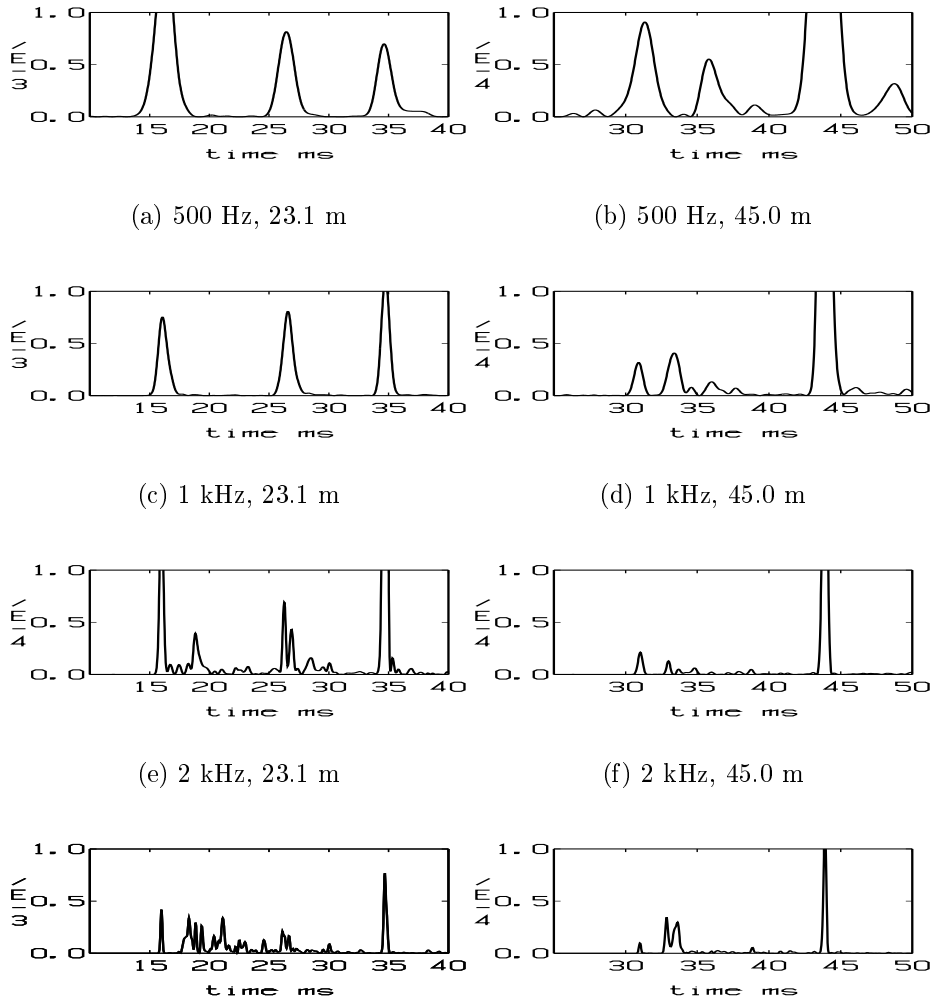

(a) 500 Hz, 23.1 m

(b) 500 Hz, 45.0 m

(c) 1 kHz, 23.1 m

(d) 1 kHz, 45.0 m

(e) 2 kHz, 23.1 m

(f) 2 kHz, 45.0 m

(g) 4 kHz, 23.1 m

(h) 4 kHz, 45.0 m

Figure 5.2: The envelope of the recorded time-series at offsets 23.1 (left column) and 45.0 m (right column) for 0.5, 1, 2 and 4 kHz Ricker pulses. Transmission loss is obtained by taking 10log of the vertical axis. Note the 10 dB differences in scaling of axes.

In looking at these pictures, it should be remembered that the arrival times t_D and t_S of the direct and the surface reflected waves are

$$\begin{array}{ll} t_D = 16.0 \text{ ms} & L_1 = 23.1 \text{ m} \\ t_S = 34.5 \text{ ms} & L_1 = 23.1 \text{ m} \\ t_D = 31.0 \text{ ms} & L_2 = 45.0 \text{ m} \\ t_S = 44.0 \text{ ms} & L_2 = 45.0 \text{ m} \end{array}$$

The late arrivals t_{21} and t_{22} are most clearly seen at the low frequencies 0.5 and 1 kHz, while the early ones are more pronounced for 2 and 4 kHz. This conforms with the fact that the penetration depth is larger for low-frequency signals in absorptive media. We also see that the direct and the surface reflected waves become more distinct at higher frequencies due to the shorter pulse length. The bottom arrivals though, exhibit a spiky appearance as the frequency increases. This is still more clear when looking at the wave amplitudes rather than the envelopes (cf. Fig. 3.3). This phenomenon may be attributed to scattering at rough boundaries and/or the presence of volume inhomogeneities.

The observed times of arrival at $L_1 = 23.1$ m and $L_2 = 45.0$ m, two at each location, suffice to determine the thicknesses and velocities of two plane layers. The result of applying the formulas (5.1) and (5.2-5) is

$$\begin{array}{ll} c_1 = 1425 \text{ m/s} & H_1 = 6.6 \text{ m} \\ c_2 = 1664 \text{ m/s} & H_2 = 10.7 \text{ m} \end{array} \tag{5.7}$$

This is a first approximation based on a minimal amount of observations. The next thing to do is to use the above layering for predictions of arrival times, and to check if they are consistent with data. Turning to the receiver at 13.2 m, we would observe reflections from the interfaces at the depths 6.6 m and 17.3 m to appear at 13.1 ms and 23.6 ms. As seen from graphs in Fig. 5.3 of data at 13.2 m this expectation is reasonably well satisfied.

6 Lateral waves

When source and receiver are both located on the interface of two different media, then the direct wave evolves in the far-field into two lateral waves whose velocities are equal to those on each side of the interface. The amplitudes decay by the inverse of the square of the horizontal range. The amplitudes are also proportional to the inverse of the difference of the square of the velocities. The waveforms resemble the Hilbert transform of the emitted pulse (apart from reversed phase of the trailing lateral wave). More will be said about lateral waves in Sec. 6.1. Fortuitously, the experimental recordings of the lateral waves turned out to be very good indeed. This fact by itself indicates that the velocity contrast at the seabottom is small. In Sec. 6.2 the lateral waves are utilized to determine the acoustical properties of the seafloor.

6.1 Some theory of lateral waves

Consider a simplified case with two half-infinite spaces $z < 0$ and $z > 0$ with acoustical parameters $\rho_i, c_i, \beta_i, i = 1, 2$. The location of the source $(0, 0, z_s)$ is assumed to be on

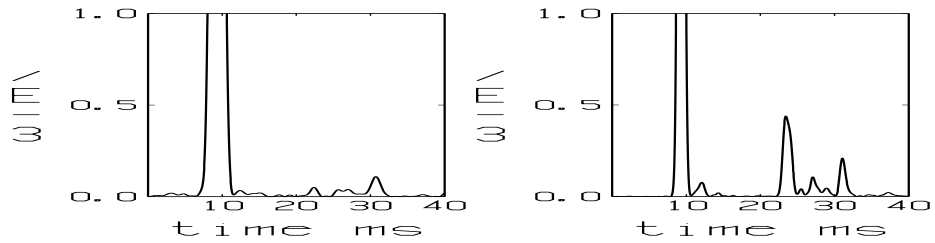

(a) 500 Hz, 13.2 m

(b) 1 kHz, 13.2 m

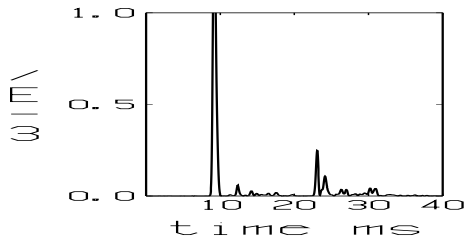

(c) 2 kHz, 13.2 m

Figure 5.3: The envelope of the recorded time-series at 13.2 m. The 10log of the vertical axis is transmission loss in dB. There is no recording of the 4 kHz Ricker pulse at this offset. The direct and surface reflected arrivals appear at 9.1 ms and 32.2 ms.

or infinitesimally close to the interface $z = 0$. Theoretically one has to distinguish between the cases

$$z_s \to 0-, \quad z_s = 0 \text{ and } z_s \to 0+ .$$

We shall mostly deal with the first case with the source in medium one just above the interface. It seems to be more in agreement with the experiment, in which the transmitter was gently descended to the seabottom.

In a cylindrical coordinate system with a vertical axis through the source position, the complex acoustic pressure $u(r, z)$ of a time-harmonic monopole source with the frequency $\omega = 2\pi f$ can be written as a Sommerfeld integral

$$u(r,z) = \frac{i}{2\pi} \int_0^\infty \frac{\rho_2}{\rho_2 k_{1z} + \rho_1 k_{2z}} e^{-ik_{1z}z} k_r J_0(k_r r) dk_r \tag{6.1}$$

where $z < 0$, and

$$k_i = \frac{\omega}{c_i}(1 + i\frac{\beta_i}{40\pi \log e}), \tag{6.2}$$

$$k_{iz} = \sqrt{k_i^2 - k_r^2}, \quad Imk_{iz} \geq 0. \tag{6.3}$$

The field for $z > 0$ is obtained by changing the exponential function in (6.1) by $exp(ik_{2z}z)$. In the formula (6.1) we have tacitly assumed that the source has approached the interface from $z < 0$. The other cases $z_s = 0$ and $z_s = 0+$ are obtained

by multiplying (6.1) by

$$\frac{\rho_1+\rho_2}{2\rho_2} \text{ and } \frac{\rho_1}{\rho_2} \tag{6.4}$$

respectively.

The wavenumber integral (6.1) was evaluated numerically for

$$\rho_1 = 1000, \quad c_1 = 1444, \quad \beta_1 = 0 \tag{6.5}$$

$$\rho_2 = 1500, \quad c_2 = 1360, \quad \beta_2 = 0.1 \tag{6.6}$$

$$f = 1000Hz, \quad -10 \le z \le 10, \quad 1 \le r \le 50. \tag{6.7}$$

The difference in transmission loss (dB) between this solution and the solution in a homogeneous whole-space is shown in Fig. 6.1.

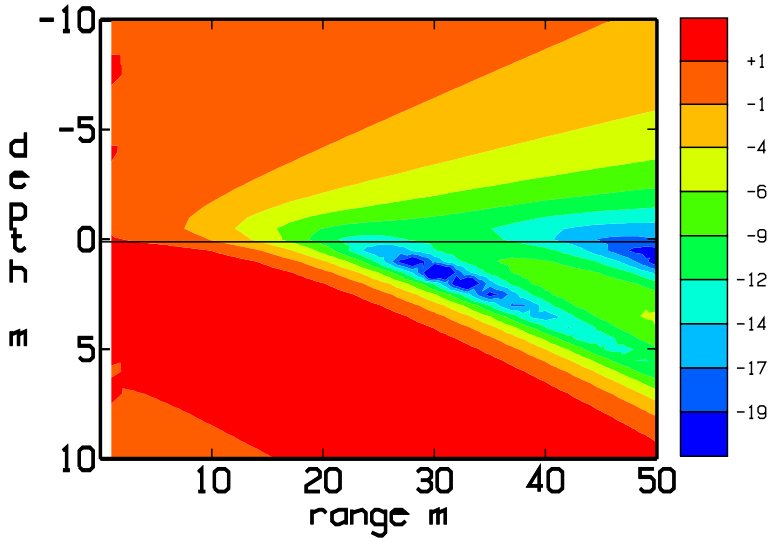

Figure 6.1: Level plot of $20\log(|u|/|p|)$, where u is the lateral wave (6.1) and p is the whole-space solution with parameters as in medium one.

A notable feature is the directivity of the response in presence of a media discontinuity. In particular, the intensity drops rapidly with range around the interface. A quantitative description of this decay can be derived from the solution (6.1) if the argument $k_r r$ of the Bessel function is large. Then, by a stationary phase argument, the integral receives its main contribution from small intervals arround $k_r \approx Rek_i, i = 1, 2$. By introducing the variables of transformation

$$k_r^2 = (1-t^2)Rek_i^2, \quad i = 1, 2 \text{ for } k_r < Rek_i$$

and

$$k_r^2 = (1+t^2)Rek_i^2, \quad i = 1, 2 \text{ for } k_r > Rek_i$$

the integrand can be developed into an asymptotic series around $t = 0$, in which the integral of the most significant term can be evaluated using the complex error function. The outcome of this asymptotic analysis is given by

$$u(r,0) \approx \frac{i}{2\pi r^2(k_2^2-k_1^2)}\left(\frac{k_1\rho_2^2}{\rho_1^2}e^{ik_1 r} - \frac{k_2\rho_1}{\rho_2}e^{ik_2 r}\right). \tag{6.8}$$

The conditions for its validity require, apart from a large $k_r r$, that the velocities are not too close. For $c_2 > c_1$, the second wave in (6.8) was derived in [15] by a different approach.

For a source located exactly on the interface and just below, this expression should be multiplied by the factors (6.4).

In contrast to the formal solution (6.1), the asymptotic form (6.8) reveals the importance of the physical parameters:

- there are two lateral waves with phase velocities equal to those on each side of the interface
- the phases of the lateral waves are opposite
- the amplitude dependences on the density contrast are different and opposite to each other
- the amplitudes decay inversely by the square of the horizontal range
- the amplitudes are inversely proportional to the difference of the square of the wavenumbers
- the amplitudes decay by the reciprocal of the frequency
- the imaginary factor i (phase advance by $\pi/2$ radians) implies that the lateral waveform will resemble a Hilbert transform of the emitted pulse

Subsequently we shall identify k_1 and k_2 with the wave numbers of the water and the seafloor. Moreover, the two lateral waves will be termed the direct water and the direct sediment wave. Fig. 6.2 (left) illustrates time traces of these waves at the point (45,0) on the interface. The media parameters (6.5-6) were applied. An examination of phases and wave amplitudes shows that the approximation (6.8) holds quite well for the center frequency. In doing this, it should be noted that only the direct sediment wave has suffered from media absorption. For informative purposes, the whole-space solution in the same point with parameters as in media one is shown in Fig. 6.2 (right).

6.2 Inversion based on lateral waves

Fig. 6.3 is a plot of the recordings at 23.1 m and 45.0 m for a 2 kHz Ricker pulse. The corresponding envelope is shown in Fig. 5.2(e)-(f) in a larger time window.

It is observed that the leading wave has traveled with the velocity of the water at the seabottom (1444 m/s). It has the characteristics of a lateral wave. The intensity drop between the receivers is -11.1 dB, well in agreement with the expected value -11.6 dB (40log(23.1/45)) for an inversely quadratic decay by range in amplitude. The waveform is similar to the Hilbert transform of the source pulse even at the shorter range 23.1 m. The sign of the phase implies that this wave has a higher velocity than the one associated with the sediment. Thus the velocity of the surface layer of the sediment is less than 1444 m/s. However, we cannot surely identify the direct sediment wave among the succeeding signals.

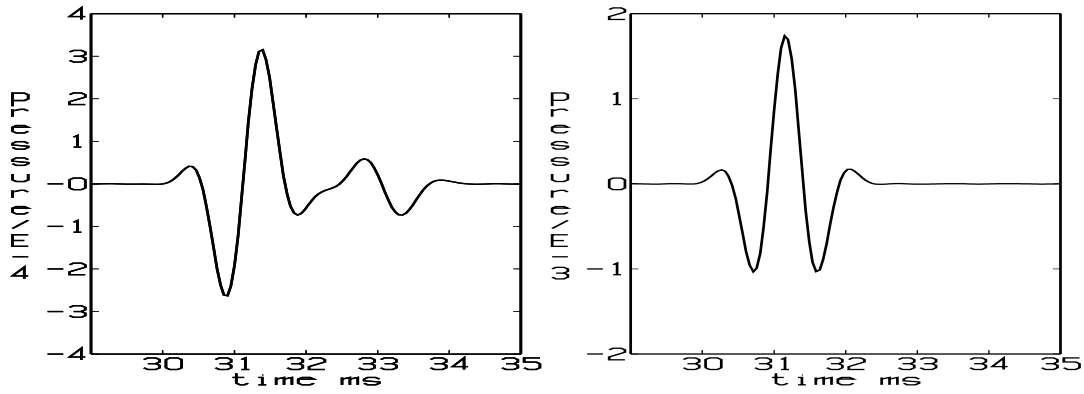

Figure 6.2: Pressure amplitude versus time of the lateral waves at the interface point (45,0) m for two half-infinite spaces (6.5-6) (left). The graph to the right show the whole-space solution in the same point for a homogeneous medium with parameters as in media one. Note the differences in waveforms and amplitudes. The center frequency of the Ricker pulse is 1 kHz.

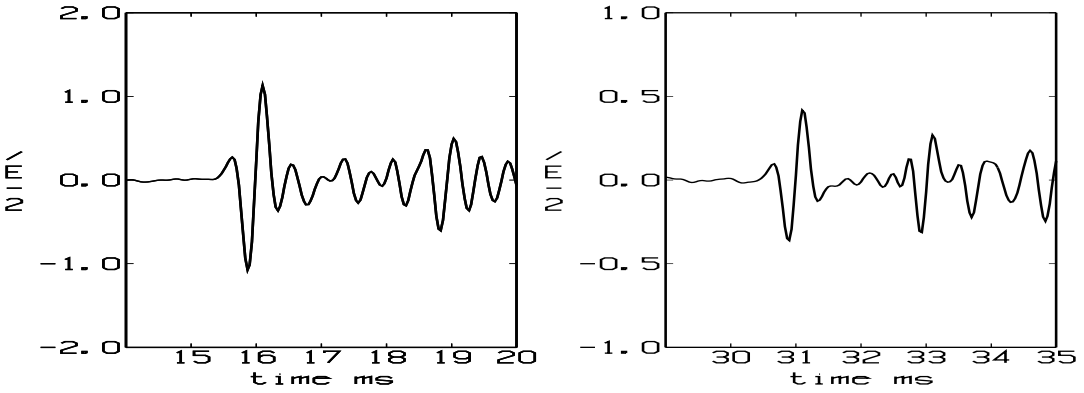

Figure 6.3: Recordings of normalized pressure amplitude versus time at the receivers at 23.1 m (left) and 45.0 m (right) for an emitted Ricker pulse of 2 kHz. Only a small time interval around the arrival times 16.0 and 31.0 ms of the direct pulse is shown.

Nevertheless, some information on its velocity can be drawn from the direct water wave. Looking at the asymptotic form (6.8), we note the amplitude factor

$$\frac{1}{2\pi r^2} \cdot \frac{k_1 \rho_2^2}{\rho_1^2 (k_2^2 - k_1^2)} = \frac{1}{2\pi r^2} \cdot \frac{c_1}{\omega \rho_1^2} \cdot \frac{\rho_2^2 c_2^2}{c_1^2 - c_2^2}$$

in the absence of absorption. Thus variations in ρ_2 and c_2 such that $\rho_2^2 c_2^2/(c_1^2 - c_2^2)$ is a constant would yield the same amplitude, at least when asymptotic theory prevails. To explore this relation, we made a series of model computations in which ρ_2 and c_2 were varied in the intervals

$$\begin{aligned} 1360 &\leq c_2 \leq 1410 \\ 1200 &\leq \rho_2 \leq 1700 \end{aligned} \tag{6.9}$$

The difference between recorded p_{r1}, p_{r2} and modeled p_{m1}, p_{m2} pressure values were taken at the 45.0 m receiver for emitted Ricker pulses with center frequencies 1 and 2

kHz. The pressure values were normalized re 1 m. The fitness function $f(c_2, \rho_2)$ was defined by

$$f(c_2, \rho_2) = 100 \cdot \frac{\int_{t_1}^{t_2} (p_{r1}(t) - p_{m1}(t))^2 + (p_{r2}(t) - p_{m2}(t))^2 dt}{\int_{t_1}^{t_2} p_{r1}(t)^2 + p_{r2}(t)^2 dt} \tag{6.10}$$

The limits of integration (t_1, t_2) was taken as (30,32.5) ms (cf. Fig. 6.2) targeting only the lateral wave at (45,0) m. The measured and modeled pulses were aligned by correlation prior to evaluation of the fitness function. Fig. 6.4 is a color map of the fitness function (6.10) as the parameters c_2 and ρ_2 range over the box (6.9).

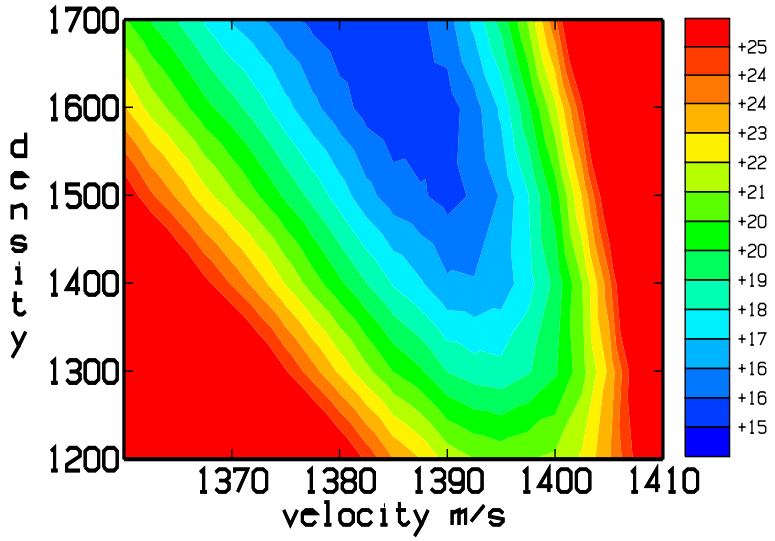

Figure 6.4: Level plot of the fitness function $f(\rho_2, c_2)$ as defined in (6.10).

We see that the best fit is roughly assumed along a valley between the (c_2, ρ_2) points (1380,1700) and (1395,1400). Despite this indeterminacy, the bounds of the velocity are narrow. This is due to the extraordinary sensitivity of the amplitude to variations in velocity when the velocity contrast is small. With the velocity in range 1380-1395 m/s the direct sediment wave would arrive at 23.1 m at 16.6-16.7 ms and at 45.0 m at 32.3-32.6 ms. Returning to the graphs in Fig. 6.3, we see a signal at 16.6 ms at 23.1 m that might be interpreted as a lateral wave with a reversed phase relative the water wave. Fig. 6.5 is the corresponding graphs for the 4 kHz case. Again we note a signal at 16.6 ms with the shape of a lateral wave.

Encouraged by the good agreement between models and observations we we shall adopt

$$c_2 = 1390 \text{ m/s}, \quad \rho_2 = 1500 \text{ kg}/m^3$$

as representative values of the velocity and density at the top of the sediment. The density estimate was read from Fig. 6.4 as the best fit along the vertical $c_2 = 1390$. It remains to determine the absorption β_2. An estimate can be obtained as follows. The ratio of the amplitudes of the two lateral waves in (6.8) are given by

$$\frac{k_2 \rho_1^3}{k_1 \rho_2^3} e^{-Imk_2 r} \tag{6.11}$$

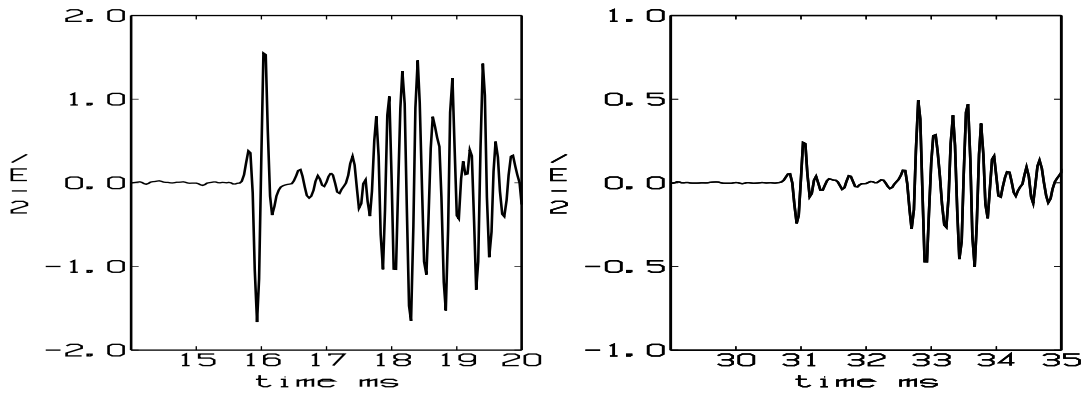

Figure 6.5: Recordings of normalized pressure amplitude versus time at the receivers at 23 m (left) and 45.0 m (right) for an emitted Ricker pulse of 4 kHz. Only a small time interval around the arrival times 16.0 and 31.0 ms of the direct pulse is shown.

The corresponding amplitude ratios in data at 23.1 m for 2 and 4 kHz are 0.17 and 0.11. By substituting the values

$$\begin{aligned} c_1 &= 1444, \quad \rho_1 = 1000 \\ c_2 &= 1390, \quad \rho_2 = 1500 \\ r &= 23.1, \quad f = 1 \text{ and } 2 \text{ kHz} \end{aligned}$$

into (6.11), and equating these ratios with the observed ones, α_2 is found to be

$$\begin{aligned} \beta_2 &= 0.16 \text{ dB}/\lambda, \quad f = 2 \text{ kHz} \\ \beta_2 &= 0.14 \text{ dB}/\lambda, \quad f = 4 \text{ kHz} \end{aligned}$$

for which $\alpha_2 = 0.15$ dB/λ is a good mean.

In summary, inversion based on lateral waves alone has resulted in the acoustical parameters

$$c_2 = 1390 \text{ m/s}, \quad \rho_2 = 1500 \text{ kg}/m^3, \quad \beta_2 = 0.15 \text{ dB}/\lambda \tag{6.12}$$

of the seafloor.

This inversion result has good viability due to the long wave interaction time with the surface layer of the sediment. In particular, the accuracy of the velocity should be within ± 5 m/s because the velocity is determined by an observed arrival time. The density and absorption predictions rely on amplitude fits, which are affected by inaccuracies both in modeling and measured data. This uncertainty may amount to ten percent. Model predictions based on the seafloor parameters (6.12) are shown in Figs. 7.3 and 7.4. As can be seen, the shape of the the direct water wave is well reproduced by the model.

The inversion result (6.12) implies that the characteristic impedance of the seafloor is $\rho_2 c_2 \approx 2.1 \cdot 10^6$. This estimate can be assessed against observations of the reflective properties of the seafloor. For that purpose, with the transmitter and receiver both at the bottom, we need to consider the wave that has undergone two air/water reflections and one bottom reflection. At the receiver at 45.0 m such a ray has a travel time of

69.1 ms and the geometrical loss is 40.3 dB. The angle of incidence towards the bottom is 24°, and using the parameters (6.12) the reflection loss at the bottom becomes 15.0 dB. Thus we anticipate a total loss of 55.3 dB at the receiver at 45.0 m. Fig. 6.6 is a plot of the envelopes of the recordings between 67 and 72 ms for the 1 and 2 kHz sources.

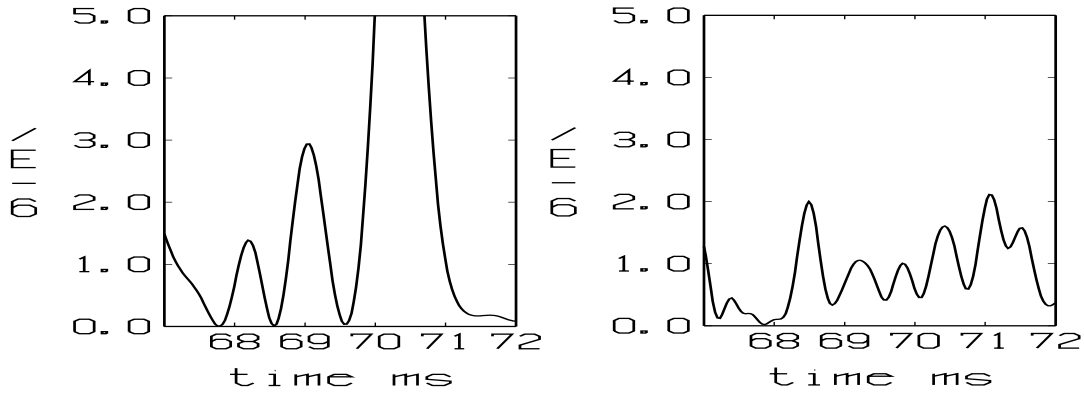

Figure 6.6: Recordings of the envelopes for emitted Ricker pulses of 1 kHz (left) and 2kHz (right) at the 45.0 m receiver.

The total loss can be read from the arrival at around 69 ms by taking 10log of envelope values. They amount to 55.5 and 60.0 dB in the 1 and 2 kHz case respectively. The first one agrees with the predicted loss, while the signal is weaker for the 2 kHz source.

7 Inversion by inference

Sometimes a specific feature can be identified by piecing together a number of clues. Besides observational evidence, information from other studies may be integrated as well. This process may result in a partial description, that could serve as a basis (model order) for fitting model predictions to measurements (matched field approach). Providing a good initial approximation makes it easier to perform the search for the remaining parameters. In this study the intention was to supplement layer thicknesses and velocities obtained in Sec. 5. by a comprehensive search for densities and absorption coefficients. The main tools would be the Genetic Algorithm (GA) and a wave propagation code based on ray tracing. Unfortunately, this effort became fruitless due to reasons that will be discussed in Sec. 7.1.

In Sec. 7.2 we present convincing evidence of the presence of a sound channel at the surface of the top sediment. In Sec. 7.3 the density and absorption of the deep sediment are estimated by a conclusive examination of particularly selected echoes. In Sec. 7.4 we illustrate graphically comparisons between measurements and model predictions based on the final inversion result.

7.1 Matched field inversion

In Secs. 5 and 6 we made use of the first three pulse arrivals of the data to construct a first approximation of the seabed at the test site. The first arrival, the direct or lateral

wave, was used for estimating the sound velocity, density and attenuation on top of the seabed. The second and third arrivals gave us an estimate of the mean-velocities and thicknesses of the first two sediment layers. In order to achieve a better resolution of the vertical structure of the seabed one should incorporate a larger time window in the analysis and try to match not only the arrival times but also the amplitudes of distinct pulse arrivals. As a result the size of the optimization problem increases and some kind of automated inversion by search algorithms will be needed.

At FOI Genetic Algorithms (GA) have been used for several years now for inverting sediment parameters from transmission loss (TL) data recorded from CW-sources, see for example [16, 17, 18, 4]. In those applications we defined the object function (which gives a measure of the model-data mismatch) to be the rms-error between computed and observed values of the TL of the pressure in dB. The summation was done over the total number of observations, which included a number of frequencies, receiver depths and receiver ranges.

In our present study we tried to use an analogous form of the object function, i.e. we defined the model-data mismatch as the relative rms-error between computed and observed values of the normalized signal envelope for pre-selected time windows which depended on the frequency and receiver range under consideration. This definition turned out to be insufficient for guiding the GA in the relevant directions of the search space. We observed three main difficulties:

- Some sort of weighting function must be introduced in the object function. In matching of transient signals the weak pulses are as important as the strong ones since their travel times contribute to the determination of the sound velocities and thicknesses of the layered media, especially to the determination of the attenuation of the media. Without weighting the GA matches the strongest pulse response and is unable to come any further in the optimization.

- The pointwise comparison between model and data makes the object function extremely sensitive to the exact arrival time of the pulse. A minor change in the modeled arrival time can significantly change the fitness-value and thus mislead the GA, even if the pulse arrivals are weighted in a reasonable manner.

- Even if the arrival times are matched perfectly, the pointwise comparison between model and data makes the object function extremely sensitive to the exact pulse widths of the signals. This can again mislead the GA in the exploration of the search space.

An appropriate object function should rather be based on the relative differences of the integrals of the computed and measured signal envelopes over adaptively chosen subintervals of the time window rather than the pointwise computed differences we tried above. Because of lack of time we have not yet managed to construct a better suited object function to this type of inversions. This should, however, be a topic of future research because of the great potential offered by the GA: we have incorporated the ray-tracing code RAY-I in our GA, which is implemented on a PC-cluster

consisting of about 20 nodes, and it executes several thousands of model runs per hour.

7.2 The velocity profile of the top sediment

In Sec. 5.2 it was found that the average velocity of the top sediment is 1425 m/s. On the other hand, the analysis of lateral waves in Sec. 6 gave a sediment velocity of 1390 m/s at the seafloor. It implies that the velocity varies by depth. This is also supported by further observations. One indication is that the bottom reflection loss for waves incident from the water depends on the frequency. Crudely, we observe a loss of 10, 15 and 20 dB for 0.5, 1 and 2 kHz Ricker pulses respectively. Bottom scattering strength measurements in the same area were reported in [2]. It was found that the bottom is smooth with a roughness of the order of a few centimeters. Therefore surface scattering is hardly the main reason for large variations of reflection loss for frequencies less then 2 kHz. Rather this phenomenon is caused by an appreciable increase of the impedance by depth of the surface layer of the sediment. Fig. 7.1 shows the recordings at the reference hydrophone within a time window 3-11 ms. The echo at 9.5 ms is the reflection from the interface at 6.6 m. The leading peaks are likely caused by the platform of the transmitter and the reference hydrophone. Since this disturbance seems to cease around 5 ms, the echo at 7.5 ms signifies a reflection within the sediment. The depth of this reflector is 5.2 m based on a uniform velocity of 1390 m/s. It implies that the velocity between 5.2 and 6.6 m is 1575 m/s. The amplitude of the echo at 7.5 ms corresponds to an impedance contrast 2.4/2.1. For constant density it would imply a change of velocity from 1390 to 1588 m/s, well in parity with the previously assumed 1575 m/s.

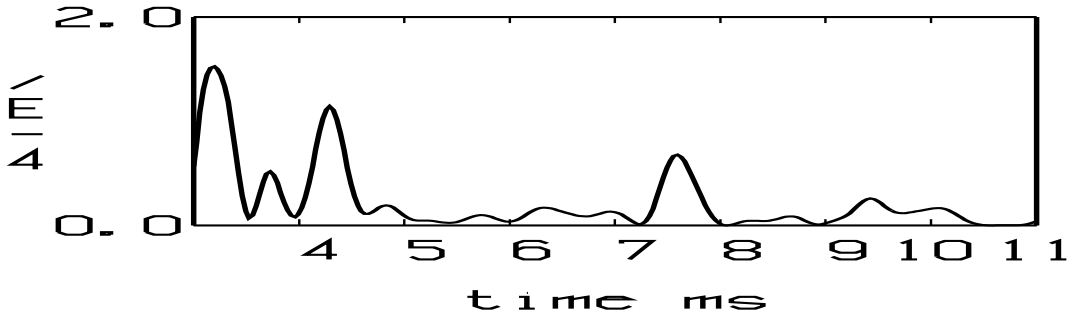

Figure 7.1: The signal envelope of the 2 kHz Ricker pulse at the reference hydrophone for the time window 3-11 ms. The arrivals before 5 ms are probably corrupt.

Looking at Fig. 5.2(h) we see a remarkably strong signal at 33 ms corresponding to a velocity of 1390 m/s for a path via a reflection at the depth of 5.2 m. The anticipated loss due to geometrical spreading and absorption is 53 dB. The observed loss is 45 dB. An immediate explanation is that cylindrical spread has set in due to transmission in the sediment sound channel.

Lacking further information on the velocity distribution, our final estimate is the piece-wise iso-speed profile

$$c_1 = \begin{cases} 1390 \text{ m/s} & 0 < z < 5.2 \text{ m} \\ 1575 \text{ m/s} & 5.2 < z < 6.6 \text{ m} \end{cases} \tag{7.1}$$

7.3 Density and absorption of the deep sediment

The density and attenuation on top of the seabed were estimated to 1500 kg/m^3 and 0.15 dB/λ respectively by analysis of the lateral wave in Sec. 6.2. We assume that these values are constant down to the interface at 6.6 m, i.e.

$$\rho_1 = 1500 \text{ kg}/m^3, \, \beta_1 = 0.15 \text{ dB}/\lambda \quad 0 < z < 6.6 \text{ m} \, . \tag{7.2}$$

The high amplitude of the first sediment arrival at the remote receiver at 45.0 m indicates that the absorption is hardly larger than 0.15 dB/λ.

For the determination of the density and absorption of the deep sediment we select two arrivals at the reference hydrophone whose amplitudes are particularly sensitive to variations in these parameters. For the density estimate we take the reflection of the 2 kHz signal from the interface at 6.6 m. This signal is shown in Fig. 7.1. The arrival time is 9.4 ms and the transmission loss (TL) is about 46.0 dB. We have run the ray-tracing code RAY-I for different values of the density ρ_2 in the deep sediment, keeping all other parameters fixed. The computed TL of this signal as function of ρ_2 is shown in Tab. 7.1.

ρ_2 [kg/m^3]	Transmission Loss [dB]
1500	56.7
1600	50.0
1700	46.4
1800	44.0
1900	42.3
2000	40.9

Table 7.1: Transmission loss of the computed sediment signal which corresponds to the arrival at 9.4 ms in the data (Fig. 7.1) for different values of the density in the deep sediment layer. The measured TL is 46.0 dB.

From Tab. 7.1 we deduce that $\rho_2 = 1700$ kg/m^3 is a good candidate for the density of the deep sediment.

In order to estimate the attenuation of the deep sediment we select the arrival at the reference hydrophone of the reflection from the bedrock interface at 17.3 m. The arrival time is 20.9 ms and the measured TL is 41.7 dB, see Fig. 7.2. The corresponding TL computed by RAY-I for varying attenuation β_2, while all other parameters are kept fixed, is shown in Tab. 7.2. We conclude that the size of the attenuation in the deep sediment layer should be about $\beta_2 = 0.1$ dB/λ.

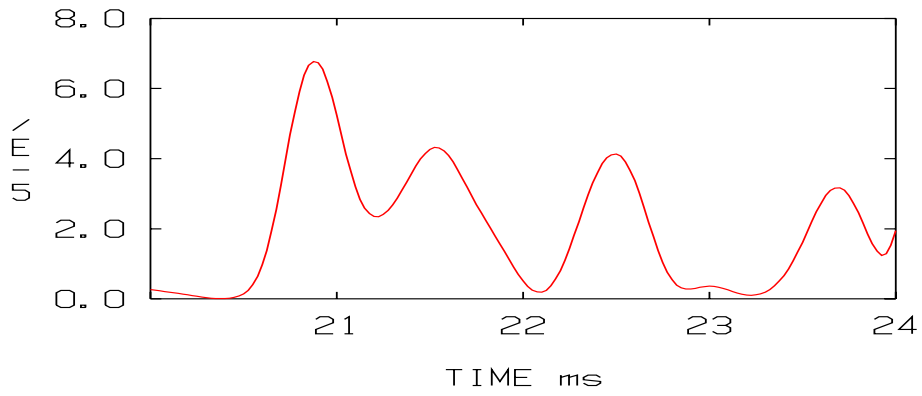

Figure 7.2: The signal envelope of the 2 kHz Ricker pulse at the reference hydrophone for the time window 20-24 ms. The maximum at 20.9 ms corresponds to the reflection from the bedrock.

β_2 [dB/λ]	Transmission Loss [dB]
0	38.4
0.1	41.0
0.2	43.6
0.3	46.1
0.4	48.7
0.5	51.3

Table 7.2: Transmission loss of the computed bedrock-reflected signal which corresponds to the arrival at 20.9 ms in the reference hydrophone in Fig. 7.2 for different values of the attenuation in the deep sediment layer. The measured TL is 41.7 dB.

7.4 Assessment of the inversion results

In this section the fullfield model XFEM is run on the seabed-configuration that resulted from the inversion analysis above, i.e.

$$c_1 = \begin{cases} 1390 \text{ m/s}, & 0 < z < 5.2 \text{ m} \\ 1575 \text{ m/s}, & 5.2 < z < 6.6 \text{ m} \end{cases}$$

$\beta_1 = 0.15$ dB/λ
$\rho_1 = 1500$ kg/m^3
$H_1 = 6.6$ m

$c_2 = 1664$ m/s
$\beta_2 = 0.10$ dB/λ
$\rho_2 = 1700$ kg/m^3
$H_2 = 10.7$ m

The sound velocity profile of the water is shown in Fig. 2.2(b). The computed field is compared to the recorded data below.

Fig. 7.3 shows the 4 kHz signal at the most remote receiver hydrophone. We see that the data signal is dominated by pulse trains of reflexes that probably arise from scatterers of unknown origin in the seabed. The late reflections are hardly visible due to strong scattering effects.

However, the distinct reflexes from the interfaces in the model agree fairly well with data. The misalignment in the arrival time of the surface reflected pulse could depend on a larger water depth at the receiver.

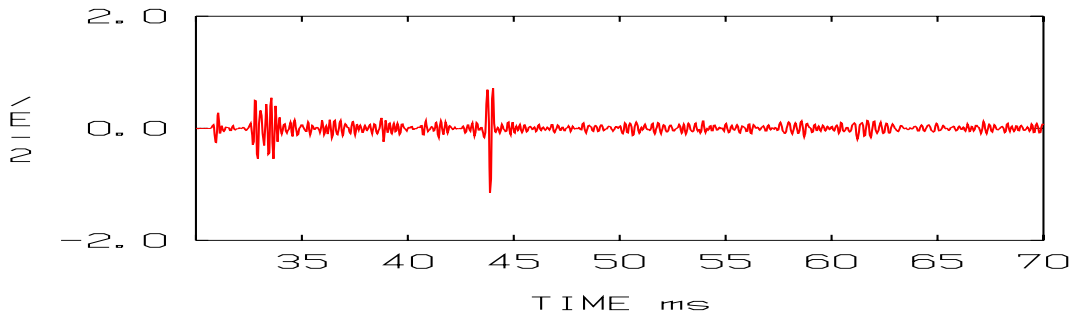

(a) Recorded signal.

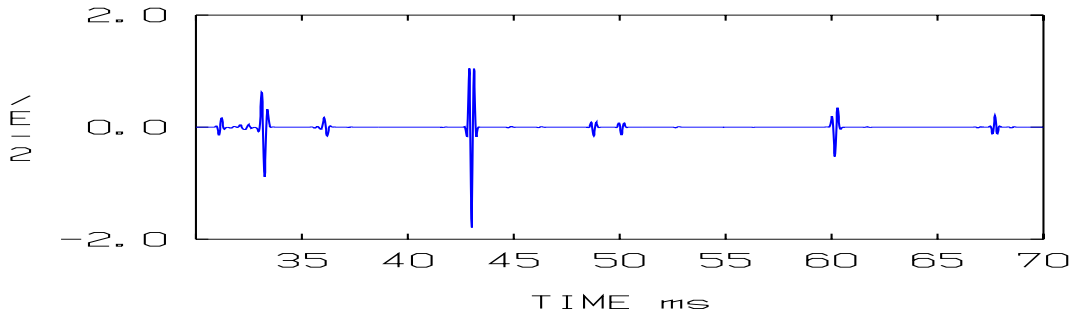

(b) Modeled signal.

Figure 7.3: Recorded and modeled signals at distance 45.0 m and center-frequency 4 kHz. The signals are normalized by the peak-amplitude of the reference signal 1 m from the source.

In Fig. 7.4 both the original signal and its envelope are displayed for the 2 kHz-case at 23.1 m. We have good agreement in the arrival times for the echoes from the sediment interfaces (18.6 and 26.4 ms). The amplitudes of the computed lateral wave and the echo from the second interface (the bedrock) agree fairly well with data. The large difference in the amplitude of the first echo is likely due to a too large impedance contrast at the interface between the two sediments. With a more refined inversion technique it could be possible to find a smoother transition between the layers.

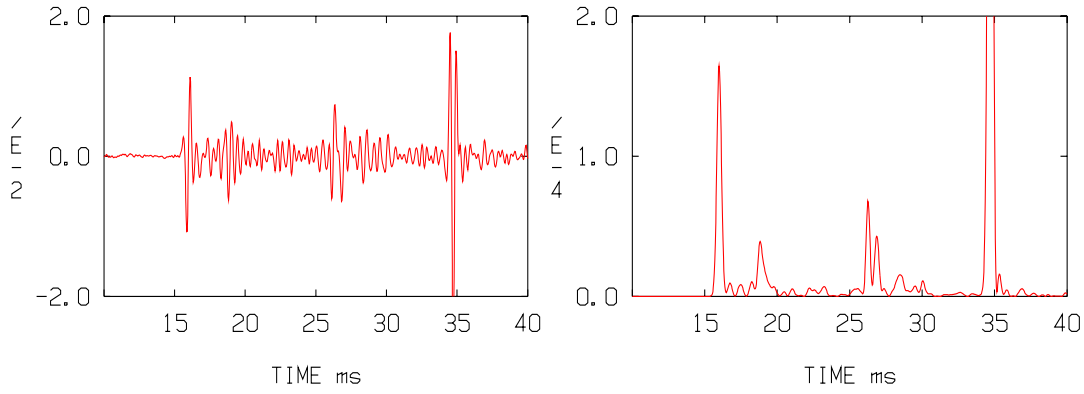

(a) Recorded pressure (left) and signal envelope (right).

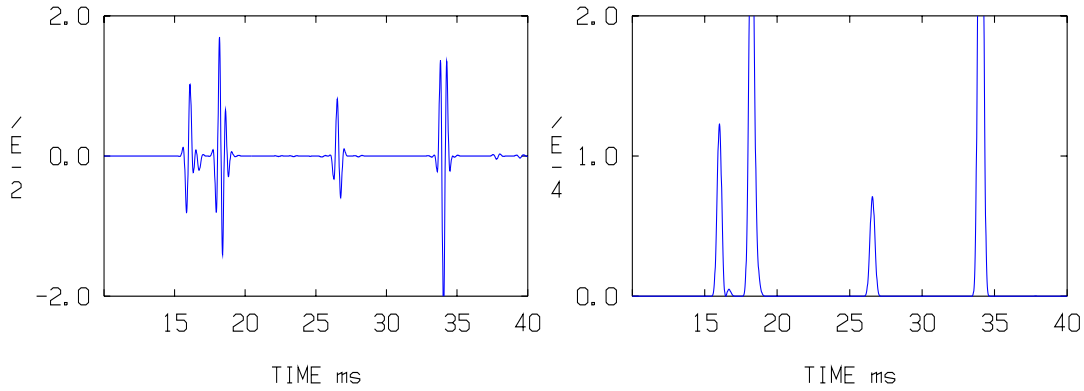

(b) Modeled pressure (left) and signal envelope (right).

Figure 7.4: Recorded (red) and modeled (blue) normalized pressure amplitudes versus time at the receiver at 23.1 m (left). The signal envelopes of the pressure pulse at 23.1 m (right). The center frequency of the Ricker pulse is 2 kHz. The direct and the surface reflected waves appear at 16.0 and 34.5 ms respectively.

Fig. 7.5 shows the signal envelope of the response to a 2 kHz Ricker pulse in the reference hydrophone. The arrival times for the echoes from the interfaces at depth 5.2 and 6.6 m respectively (7.5 and 9.4 ms) agree well with data while the echo from the bedrock (20.9 ms) departs with about 1 ms. It should be remembered, however, that the inversion was based on data in the remote receivers.

The amplitudes of the second and third arrivals agree well with data because they were the target of the inversion of the density and attenuation of the deep sediment.

We have no explanation for the remaining arrivals in the data.

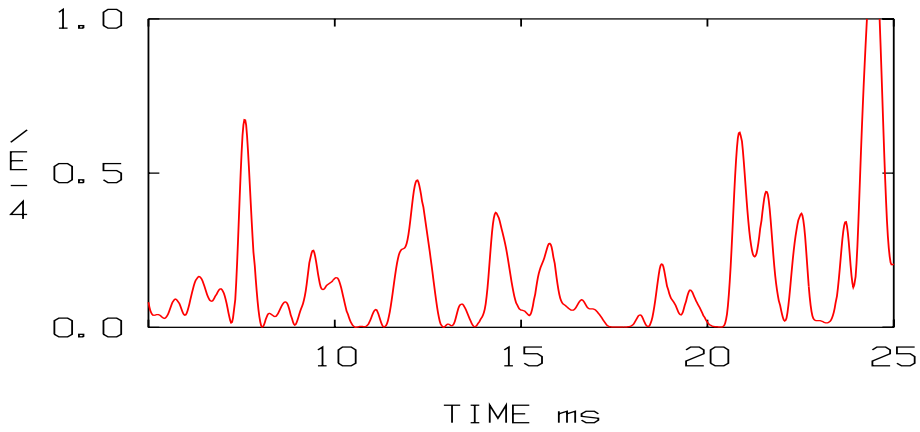

(a) Recorded signal.

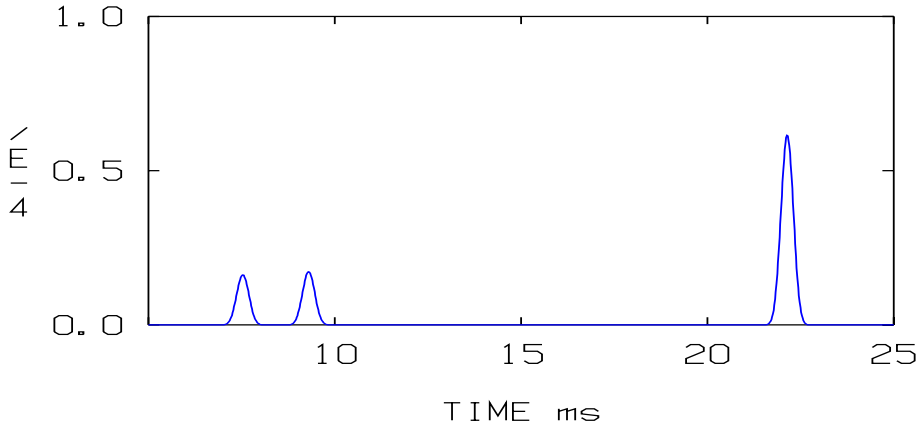

(b) Modeled signal.

Figure 7.5: Recorded and modeled signal envelopes at the receiver hydrophone. The center-frequency of the Ricker-pulse is 2 kHz. The signals are normalized by the peak-amplitude.

Finally, in Fig. 7.6 the time-series of a 500 Hz signal at 45.0 m is shown. The reflection from the first sediment interface (32.9 ms) in the model is so strong that it dominates the direct wave. The echo from the bedrock interface (36.0 ms) is well reproduced. The echo around 50 ms corresponds to a wave that has traversed both the water column and the first sediment, and that around 60 ms corresponds to a wave that has reflected both the water surface and the bedrock interface.

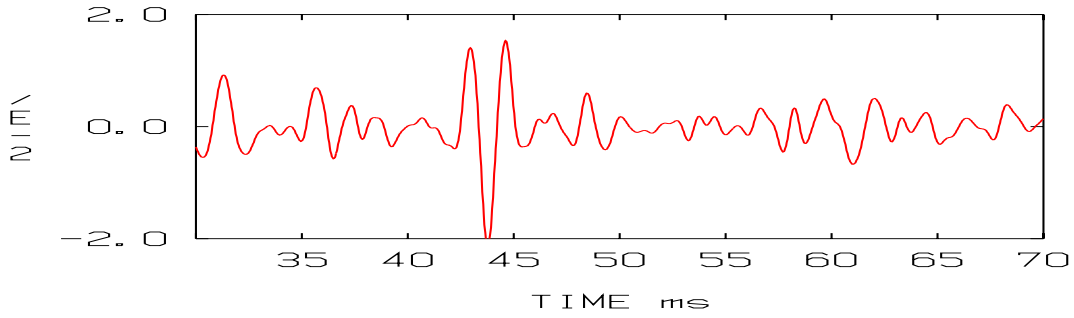

(a) Recorded signal.

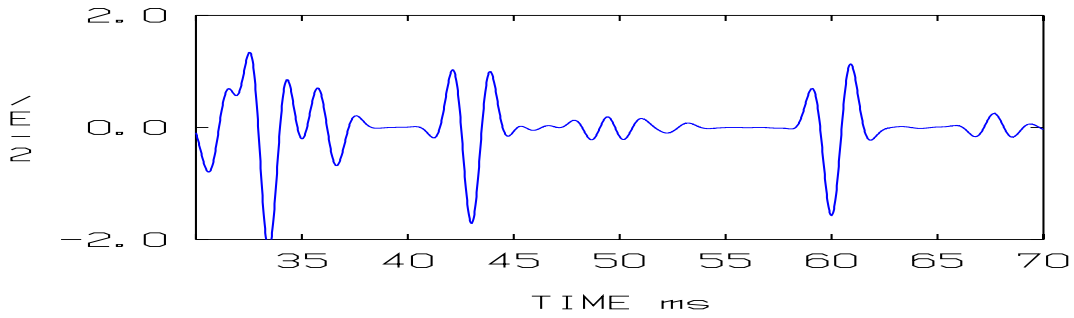

(b) Modeled signal.

Figure 7.6: Recorded and modeled signals at distance 45.0 m and center-frequency 500 Hz. The signals are normalized by the peak-amplitude of the reference signal 1 m from the source.

8 Concluding remarks

The Ricker pulses centered at 1,2 and 4 kHz were adequate for the exploration of the top layer. In particular the recordings of the lateral waves were excellent. However, deep returns show almost a continuous train of reflections with unknown origin. It would be interesting to describe and, if possible, to identify features of scatterers with respect to separation range and frequency, the two parameters for which measurements are available. Such a study should be accompanied by development of modeling tools to deal with multifaceted scattering phenomena.

Probing by frequencies less than 500 Hz is more adequate for exploration of large-scale features beyond a depth of some ten meters. The scattering would be of minor importance, and the present computational models would do. The problem is rather provisions of equipment for low-frequency transmission and calibration in shallow waters.

This work shows that acoustical properties of the seafloor can be gained from lateral waves. Their amplitudes are quite sensitive to source-receiver range, frequency and the velocity contrast at the seabottom. Since the latter is unknown prior to the experiment, it might be difficult to obtain good measurements. In any case such experiments should

be supplemented by a study of the bottom reflection coefficient of incident waves from the water. Its variation by frequency embodies information of the upper part of the seabed. The simplicity of this experiment is of interest to REA.

The presence of a sediment sound channel around the seafloor raises further questions. First, is this a local phenomenon or is it typical for this environment. Second, what is the propagation range for sediment guided high frequency (4-8 kHz) Ricker pulses. Our results indicate it could be as large as 100 m.

Basic to any search algorithm is a suitable formulation of the fitness function, which provides a quantitative assessment of the model result for a given set of parameters. The design of the fitness function for transient signals must allow for some relaxation in time arrivals, in particular for time pulses less than 1 ms. For optimization in the time-domain this is an important topic for further research.

Acknowledgement

Per Söderberg was the chief conductor of the field experiment.

Ulf Skotte and Göran Stensson carried out thousands of practicalities during the field work.

Stefan Ban, Peter Lindqvist and Torbjörn Ståhlsten performed a thorough testing and calibration of the sonar equipment.

Lars Lekzén prepared both the design and electronics of the transmitter platform.

Jörgen Pihl shared his eminent knowledge on many occassions.

Capt. Jonnie Tvinnhagen and his crew is acknowledged for the great hospitality and assistance onboard HMS Urd.

References

[1] S. Ivansson, M. Levonen, and P. Söderberg. Quantitative Determination of Sediment Properties in the Baltic Using Close-Range Seismic Reflection Data. Methodology report FOA-R-00-01555-409–SE, 2000.

[2] E. Dalberg, M. Levonen, B. Nilsson, M. Olsson, J. Pihl, and P. Söderberg. Geoacoustic Sediment Properties in the Baltic. Methodology report FOA-R-00-01466-409–SE, 2000.

[3] L. Crona, P. Krylstedt, J. Mattsson, A. Olsson, and M.Tulldahl. Environment assessment for underwater sensors in the Stockholm archipelago, part 2 - optical transmission and inversion of electromagnetic sub-bottom parameters. User report FOI-R–0707–SE, 2002.

[4] L. Abrahamsson and B.L. Andersson. Inversion of seabed parameters in the Stockholm archipelago. Methodology report FOI-R–0300–SE, 2001.

[5] I. Karasalo and J. Mattsson. Transient scattering from submerged objects - theoretical predictions and experimental results. Tech. Rep. FOA-R-99-001169-409–SE, 1999.

[6] M.J. Beran and G.B. Parrent Jr. *Theory of Partial Coherence.* Prentice-Hall, 1964.

[7] G.L. Maynard, G.H. Sutton, D.M. Hussong, and L.W. Kroenke. The seismic wide angle reflection method in the study of ocean sediment velocity structure. In *Symp. on Physics of Sound in Sediments, ed. L. Hampton*, pages 89–117, Austin, Texas, 1973.

[8] J. Pihl and L. Abrahamsson. MODELOSS - A User Oriented Code for Transmission Loss Calculations. FOA report R-95-00173-2.2-SE, 1995.

[9] L. Abrahamsson, S. Jahnberg, J O Johansson, P-A Karlsson, and K. Ohlson. Modellering av antitorped-torped i simuleringsmodellen MUMS. Metodrapport FOI-R-0219–SE, 2001.

[10] L. Abrahamsson and B.L. Andersson. NLAYER - An ELFE code for horizontally stratifed media. Tech. Rep. FOA-R-97-00586-409–SE, 1997.

[11] S. Ivansson and I. Karasalo. A high-order adaptive integration method for wave propagation in range-independent fluid-solid media. *J. Acoust. Soc. Amer.*, 92:1569–1577, 1992.

[12] I. Karasalo. Exact finite elements for wave-propagation in range-independent fluid-solid media. *J. Sound Vib.*, 172:671–688, 1994.

[13] C.H. Green. Velocity determinations by means of reflection profiles. *Geophysics*, 3:295–305, 1938.

[14] C.H. Dix. Seismic velocities from surface measurements. *Geophysics*, 20:68–86, 1955.

[15] L. Brekhovskikh and Yu. Lysanov. *Fundamentals of Ocean Acoustics.* Springer-Verlag, 1982.

[16] J. Pihl, P. Söderberg, A. Wester, and V. Westerlin. A Method for On-site Determination of Geoacoustic Parameters. Methodology report FOA-R-99-01281-409-SE, 1999.

[17] B.L. Andersson. Analysis of transmission loss data with JEPE-S and a genetic algorithm. Methodology report FOA-R–01375-409–SE, 1999.

[18] L.Abrahamsson and B.L. Andersson. Identification of seabed geoacoustic parameters from transmission loss data. Methodology report FOA-R-00-01752-409–SE, 2000.